EVLA Memo 214
Determining the VLA Antenna Elevation Gain Dependences

Rick Perley

January 11, 2022

Abstract

We describe in detail the methods which have been developed for determining the VLA antennas' elevation gain dependence. Results show little difference in elevation gain between polarizations, or within the 1-GHz width of an individual IF tuning. However, there are very significant differences in the gain-elevation dependencies between bands, and smaller, but significant, differences between opposite ends of the K and Ka bands.

1 Introduction

The VLA antennas have a strong dependence of forward gain with elevation, due to a combination of effects. The primary cause is an elevation-dependent misorientation of the subreflector w.r.t. the main reflector. As described in EVLA Memo 211, this can be largely offset – for feeds located near the horizonal axis of the cassegrain feed ring – by a suitable elevation-dependent rotation of the subreflector. Although this greatly reduces the loss of gain, there remains a significant residual dependency of the antenna gain on elevation. This is a repeatable effect, so can be corrected for in software once the gain dependency is determined.

Determination of the elevation gain dependency is straightforwards. The simplest method is to track a strong point source from low to high elevation (or vice versa), at the various bands, and measure the elevation dependence of the antenna gains. As this takes up a significant amount of array time, a more efficient method is to utilize an existing observational program which includes one or more calibrator sources over a wide elevation range at all the relevant bands.

Such an observational program is the 'flux density program'. We have, since 1983, observed a suite of standard flux density sources, usually for 24 – 30 hours, in order to measure, and to track, their flux densities, polarizations, and structures. A full description of this program, and its major results, are given in Perley & Butler (ApJS, 2013 **204**, 19, and ApJS, 2017, **230**, 7). Since this program makes multiple observations of multiple sources at all VLA observing bands, the data can be utilized for other purposes, including that of determining the elevation gains. In this memo, we describe the methods, and show the results for the most recent run, taken in September, 2021. A subsequent memo will describe the stability of these gains over time.

2 Observations

2.1 Date and Weather

The 2021 observations were taken over a 24-hour period, starting near 23:53 IAT (5:53 PM, MDT) on Sept 09, 2021. The weather was clear and dry, and the array was in the **C** configuration. Windspeeds were light throughout the run. These weather conditions meant there was a significant diurnal temperature range of over 20 degrees C. A plot of the wind and temperature is shown in Fig. 1. This large diurnal temperature change resulted in significant electronics gain variations – up to 40% in power gain for the high frequency bands – which are much larger than the elevation-dependent gains we are seeking to measure. To isolate the elevation-dependent gains, we must first remove the temperature-induced temporal gain. This is done by utilizing the switched power data, as described below in Section 3.2.

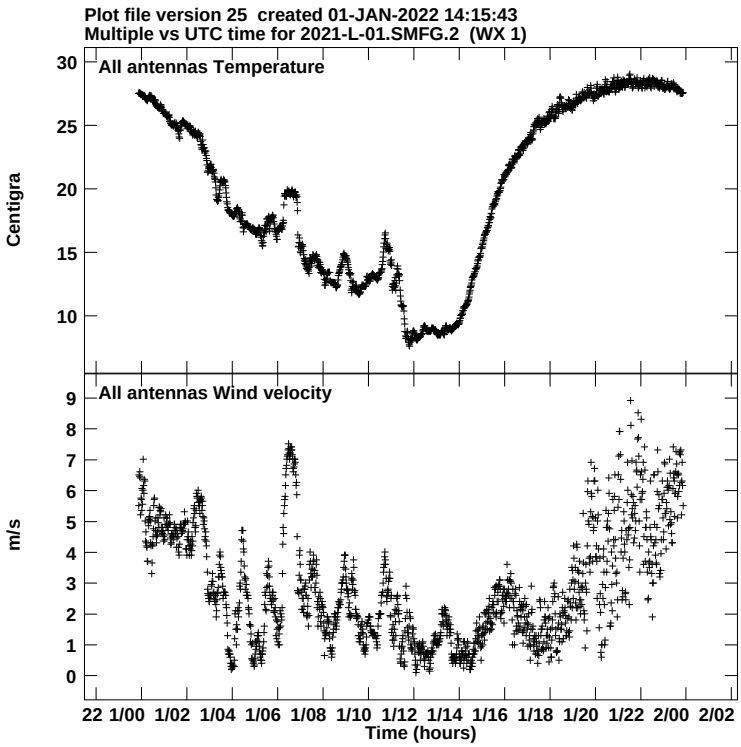

Figure 1: Showing the windspeed and temperature during the 24-hour flux density run on Sept 9/10, 2021. Winds were light throughout the observations (5 m/s = 11 miles/hr), and there was a large diurnal change in ambient temperature.

2.2 Frequencies and Bandwidths

Accurate utilization of the switched power measurements can only be done when using the 8-bit samplers[1]. This in turn limits the frequency coverage to a maximum of two 1-GHz-wide IF channels. This is no way limits the accuracy of our results, as all observed sources are strong calibrators, and we do not expect signifcant frequency structure in the elevation-gain dependency. .

The maximum bandwidth of 2 GHz means that full-band coverage is available for P, L, and S bands, while specific tunings are required for the higher frequency bands. The chosen frequencies are shown in Table 1. These were selected to avoid regions of known strong RFI[2], and to reasonably span the width of each frequency band.

2.3 Source Selection

As the primary purpose of the observations was to determine the flux densities and polarizations of the standard calibrators, the source list included 3C48, 3C123, 3C138, 3C147, 3C196, 3C286, and 3C295. Each of these was observed 6 – 8 times at all VLA observing bands, from P through Q.

The wide spread in Right Ascension of these seven standard sources, and the need to accurately determine the polarization and elevation gain curves, requires the full 24-hour duration. However, ∼6 observations for each source at each band, each for less than a minute, means only a small fraction of the 24-hour duration is utilized for these purposes. Thus, there was considerable time availble for observations of other sources for other goals. It was decided to include three to four observations each of the 24 strongest high-frequency calibrators north of $\delta = -30$ in order to determine their polarization properties. The rationale for this is that the standard methods

[1]To maximize sensitivity, the power levels to the 3-bit samplers are set quite high, resulting in a non-linear relation between the reported digital power and the true analog power.

[2]These were determined by consulting the results of the regular 'frequency sweep'. However, as these sweeps are done with the antennas pointed to the zenith, they do not include RFI from satellites associated with the 'Clarke Belt' – the zone of geosynchronous satellites which are seen to the VLA at a declination of near −4 degrees. As noted below, many of the sources observed in the 2021 run were close to this declination, and many spectral windows were lost due to satellite RFI.

Table 1: **Frequency Tunings Utilized for the 2021 Flux Densities Run**

Band	N_{SPW}	Freq. Span MHz	$\Delta\nu$ MHz
L – Lo	8	1008 – 1520	1.0
L – Hi	8	1520 – 2032	1.0
S – Lo	8	1998 – 3012	2.0
S – Hi	8	2988 – 4012	2.0
C – Lo	8	4188 – 4700	2.0
C – Hi	8	6456 – 7480	2.0
X – Lo	8	7988 – 9012	2.0
X – Hi	8	10488 – 11512	2.0
Ku– Lo	8	13488 – 14512	2.0
Ku– Hi	8	15988 – 17012	2.0
K – Lo	8	18738 – 19762	2.0
K – Hi	8	24988 – 26012	2.0
Ka– Lo	8	31488 – 32512	2.0
Ka– Hi	8	36488 – 37512	2.0
Q – Lo	8	41488 – 42512	2.0
Q – Hi	8	47488 – 48512	2.0

of deriving the antenna polarizations (by tracking strong calibrators over a wide range of parallactic angle, or observing a strong, unpolarized source) are often not applicable to high frequency observing. This is so because a large fraction of VLA observing is now of a short duration (hence no significant parallactic rotation), and the only known strong, unpolarized source at high frequencies – 3C84 = J0319+4130 – is below the elevation limits for nearly half the day. Hence, we included these 24 strong sources in the hope that one or more have sufficiently low polarization to be utilizeable as a high frequency polarization calibrator[3].

In addition to the strong high-frequency sources, we added two known low-polarization CSS sources, to accurately measure their flux densities and polarizations over the VLA bands. For these sources, and the flat spectrum sources, observations were made from L through Q bands, as they have no use as calibrators at sub-1GHz frequencies.

The important question of how strong, and how low a polarization is required for successful polarization calibration can also be answered by these observations. This result will be presented in a separate memo.

Also added to the source list were observations of the planets Venus, Mars, Uranus, and Neptune, at L through Q bands, as these are potential flux density calibrators for high frequency observations. Additionally, observations of Mars can be used to check the absolute flux density scale, as described in the 2013 P&B paper. The results for these observations will also be presented separately.

Finally, we added three northern sources used to monitor system performance, and three sources close to the Galactic center, at the behest of Lorant Sjouwerman, giving a total of 44 target sources, as listed below.

- **Standard Flux Calibrators:** J0137+3309 = 3C48, J0437+2940 = 3C123, J0521+1638 = 3C138, J0542+4951 = 3C147, J0813+4813 = 3C196, J1331+3030 = 3C286, J1411+5212 = 3C295.
- **Northern Sources:** J0217+7349, J1153+8058, J1800+7828
- **Flat-Spectrum Sources:** J0238+1636, J0319+4130 = 3C84, J0359+5057, J0418+3801, J0501-0159, J0532+0732, J0607-0834, J0609-1542, J0730-1141, J0750+1231, J0927+3902, J1058+0133, J1229+0203=3C273, J1256-0547 = 3C279, J1337-1257, J1415+1320, J1549+0237, J1642+3948 = 3C345, J1733-1304, J1743-0350, J1751+0939, J1924-2914, J2148+0657, J2253+1608 = 3C454.3.
- **Known Low-Polarization Sources:** J1407+2827 = OQ208, J2355+4950
- **Planets:** Venus (1348-1203), Mars (1150+0156), Uranus (0249+1548), Neptune (2332-0417)

[3]We are fully aware this was unlikely to succeed, as it is well known that flat or inverted-spectrum sources are both variable and significantly polarized. But we thought it worth the effort, nonetheless.

- **Others:** J1602+3326, J2225-0457, J2258-2758, J1130-1449

2.4 Observing Duration and Band Sequence

Observing 44 sources three to eight times, at eight or nine bands, requires a large number (over 1700) of band changes, each of which requires motion of the subreflector in both focus and rotation. It is thus important to minimize the time spent in moving the subreflector. The sequence of observing bands thus followed the feed horn arrangement around the cassegrain focus ring: L → X → C → S → Ku → K → Q → Ka. For the observations of the 3C sources, P-band was included, which preceded the L-band observation.

For each source, referenced pointing was done at X-band, following the L-band observation, using the source itself, except for the four planets, for which the nearest strong calibrator was utilized. The duration for this determination was set to 2m30s.

For the 3C sources, P-band was included. Because the subreflector travel time from P to L band is quite long (about 25 seconds), we elected to make the P-band observations with the subreflector set to the L-band position. This causes only a small gain loss, which is no issue since all the target sources are so strong. By doing this, about 30 seconds of time is saved for every P-band observation – over 20 minutes for this observing program. To do this, Ken Sowinski modified the 'parameters database' such that the P-band focus positions for the antennas were replaced with their L-band values[4].

Because all the sources are very strong, sensitivity is not an issue, so the time spent at each band was set so that only 15 to 20 seconds of stable data were obtained at each band for each source. For the initial observation for each source (P-band for the 3C sources, L-band for all the others), the 'on source' option in the OPT was selected, and set to 20 seconds – this bypasses the need for estimation of the time taken to move the antennas from one source to the next. For the other bands, the 'duration' option was used, and adjusted to account for the subreflector travel time. Values ranged from 20 seconds at X-band (as this followed the X-band referenced pointing observation) to 33 seconds at Ku band. The average time spent observing a source over the 8 or 9 bands, including the referenced pointing determination and the travel time needed to reach it, was about 7 minutes.

With 44 sources, 8 or 9 bands, and 3 to 7 observations per source, a total of 1713 separate observations were made. Executing this SB presents a stiff challenge for the on-line system, and has over the years uncovered a number of problems.

3 Editing and Calibration

The calibration process for these runs generally follows well-established paths, and for that reason will not be described in detail here. Below are some specialized topics of separate interest.

Because our goal is to determine the elevation gain dependency of each antenna, the data to be processed had only the default atmospheric opacity correction applied. The normal procedure of applying the previously-determined elevation gain corrections was turned off.

3.1 RFI Flagging

There is much RFI in the lower frequency bands, which must be removed before sensible calibration can be executed. For L-band, it was decided to simply purge (flag out) nine of the spectral windows: SPWs 2, 3, 4, 5, 9, 10, 11, 15 and 16, as the degree of RFI degradation is too great for sensible results to be obtained. For the retained SPWs (1, 6, 7, 8, 12, 13 and 14), sporadic RFI was removed as described below. At S-band, two spectral windows – 2 and 3 (the latter contains the Sirius-XM satellite radio signals) were removed for the same reason.

For the remaining bands, all SPWs were retained, although many of these at C, X and Ku bands required considerable flagging. All are affected by sporadic RFI, which was removed the clipping (flagging) all visibilities above a determined level. This was done by applying an initial, rough calibration based on 3C286, from which the visibility range for each source (both in parallel and cross hands) was determined. Visibilities outside these

[4]In fact, this was done correctly only for the 2019 observations. For the 2021 observations, we forgot to make this modification to the parameters database, which resulted in all L-band observations of the 3C sources being taken while the subreflector was still moving between the P and L-band positions, as only 20 seconds was allotted for the L-band observations. This prevented proper gain calibration of the L-band data. A short observation of 3C286, OQ208, and the three northern sources at L-band, was made on 15 December, 2021, to establish the proper flux densites.

ranges were flagged using `CLIP`. This is an efficient and effective method of RFI mitigation, as nearly all sources are compact and flat spectrum over the range of each IF, so determination of the boundary values was both simple and sufficient.

During this 'clipping' process, it was noted that some of the spectral windows in S, C, X, and Ku bands were heavily affected by RFI only for those sources near the geostationary zone. Sources north of +10 and south of −20 were much less affected. This clearly is result of the large population of geosynchronous satellites. Note also that not all directions along the geosynchrous zone are unuseable – some observations, particularly at higher frequencies where the antenna gain pattern is narrower, were not ruined by RFI, and could be retained.

3.2 Removing Diurnal Gain Changes

As noted earlier, the VLA's amplifier chains have a highly temperature-sensitive gain response, due to temperature variations in the vertex room. This can largely be removed by application of the switched power values[5].

As the observations were taken in clear dry weather, with a corresponding large diurnal temperature change, the subsequent gain changes were quite large, as shown in Figures 2 and 3, showing the measured gain changes for L through Q bands. Although all bands show a similar diurnal gain change, there are significant differences in the amplitudes of the gains.

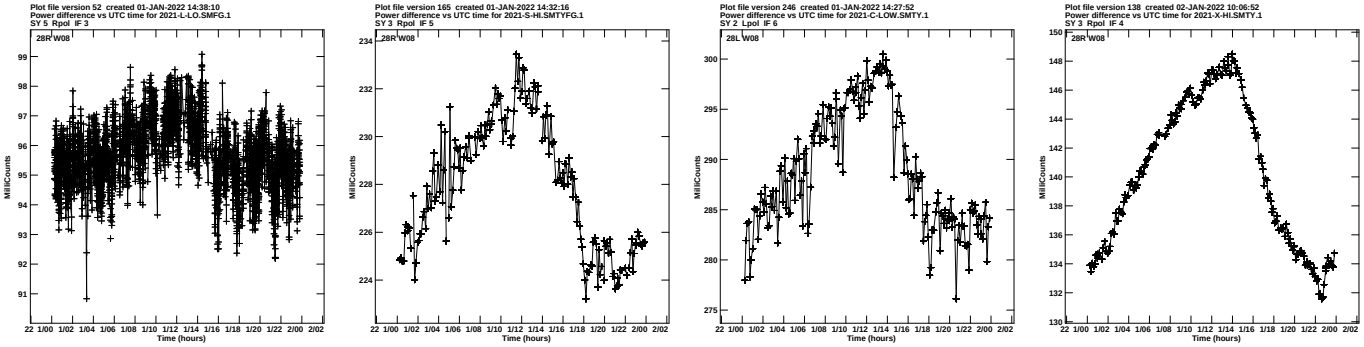

Figure 2: Showing the measured switched power on ea28 for L, S, C and X bands. The (max/min) power gain ratios for these bands is relatively small – 1.02, 1.03, 1.05, and 1.12.

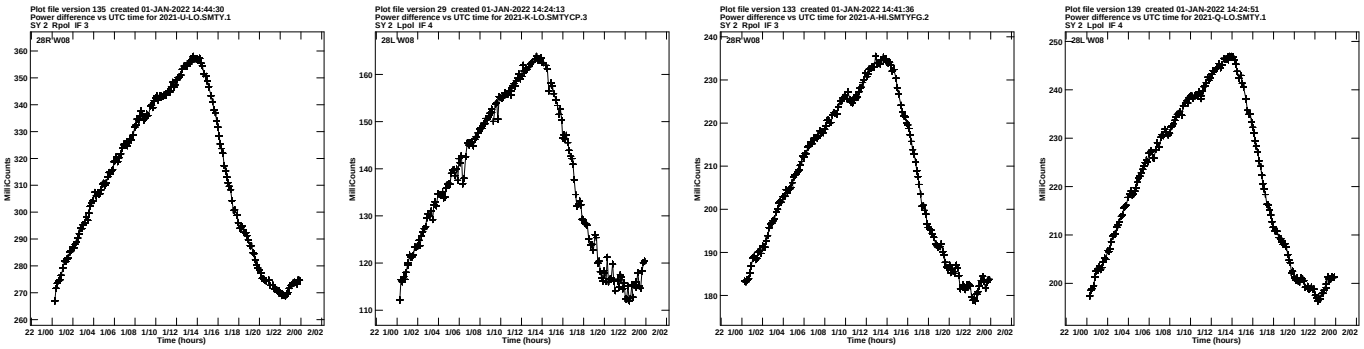

Figure 3: Showing the measured switched power on ea28 for Ku, K, Ka and Q bands. For these high frequency bands, the (max/min) gain ratios are much larger than the four low frequency bands – 1.32, 1.44, 1.29, and 1.24.

The origin of these large dirurnal gain variations is of some interest. Clearly, they are fundamentally caused by temperature sensitivity of the RF and IF components in the vertex room. However, the very different gain ratios shown in the figures indicate there is not a single component responsible. The singularly high values for the four high frequency bands strongly suggests an important component is the T303 (U-X Converter) module, which is mounted on the wall of the vertex cabin. But this is clearly not the only origin, as the low frequency

[5]Not entirely, as the noise diodes themselves have a temperature response. Studies have shown the diurnal effect can be reduced to ∼2%.

bands show similar curves, albeit with lower gain ratio. For these, the post-amps, which are directly bolted to the feeds, are a likely origin, as these four feeds all extend outwards into the night air, and thus will act as 'heat pipes'. The sheer size and mass of the L and S band feeds might then explain the greatly reduced diurnal temperature sensitivity of these bands.

The switched power ('PDif') values were applied to the data at C through Q bands, via the AIPS program 'TYAPL'. No application was done at L and S bands, as the diurnal effect is small, and the switched power values for most of the SPWs are highly corrupted by RFI[6].

3.3 Calibration

Following the operations described above, the data calibration (delays, bandpass, gains) process followed standard procedures. The flux density scale was set by the known values of 3C286, using models of that source derived from earlier A-configuration observations. Because the elevation dependency has not been removed, the amplitude scales were initially set by the single observation of 3C286 at E = 50 degrees, the fiducial gain angle.

4 Elevation Gain Determination

Following the basic calibration described above, the gain-determination program CALIB was run, using up to 30 unresolved calibrators. The resulting 'SN' table is read by the special AIPS program 'ELINT'. This program solves for the coefficients of a third order polynomial (i.e., a parabola), and the source flux densities, based on the gain values for 3C286[7]. 'ELINT' provides these coefficients for each spectral window and polarization. It can also generate the average coefficients over a specified range of SPWs.

In practice the Calibration and Gain Determination steps are usually interative, as bad gain solutions (usually due to failed referenced pointing) degrade both the overall gain calibration, and the determination of the source flux densities and subsequent gain tables. Purging bad gain solutions is straightforwards – the gain solutions provided by CALIB are reviewed, and deviant values can be flagged by hand via UVFLG, or by the program SNFLG. Typically, up to 10% of the gain solutions at the highest frequencies must be removed. Virtually all discrepant gain solutions at frequencies above 8 GHz are too high (meaning, the visibilities are too low) – as expected if due to poor pointing. It is believed that all of these are due to failed referenced pointing – either because the referenced pointing regimen failed, or because the solution determined was not actually applied to the observation. Although the former explanation is the most common, evidence for the latter has been seen in other observations.

Examples of the R and L polarization ELINT fits are shown in the following figures for antennas 4 and 15 – these were chosen as they represent both a well-behaved antenna (ea04), and a poorly-behaved antenna (ea15). Written at the top of each plot are the three voltage gain coefficients, ($G = a_0 + a_1 E + a_2 E^2$), a post-fit rms (in gain units), and the effective rms pointing error, presuming the post-fit rms is entirely due to pointing offsets. Examination of the results over the bands suggests that for Ku-band and higher, residual pointing errors, typically of $\sim 7 - 8$ arcseconds, are indeed the dominant source of error. For lower frequencies, residual gain fluctuations are the dominant source. In Figure 4 are the fits for C, X, and Ku bands. In Figure 5 are the fits for K, Ka, and Q bands.

5 Results

In the figures, the gain functions have been normalized (set to 1.0) at an elevation of 50 degrees.

ELINT can plot the data and solution fits for each of the spectral windows for a given IF tuning in a single plot, and provide the averaged coefficients. Examination of these shows the eight fits are nearly identical, as expected. Thus, the solutions utilized in the following analysis are the averaged coefficients over the eight spectral windows for both IF tunings. A discussion of the change in coefficients over the full width of a single frequency band is given in the following sections.

No fits were performed for L or S band, as examination of the solutions clearly indicated no significant elevation dependence. For X-band and higher, the *typical* gain curves (in terms of the voltage gains needed to

[6]AIPS provides clipping the smoothing processes in the program 'TYSMO', which is highly effective in removing RFI-corrupted values.

[7]There is no specific justification for a parabola, other than it gives a good fit.

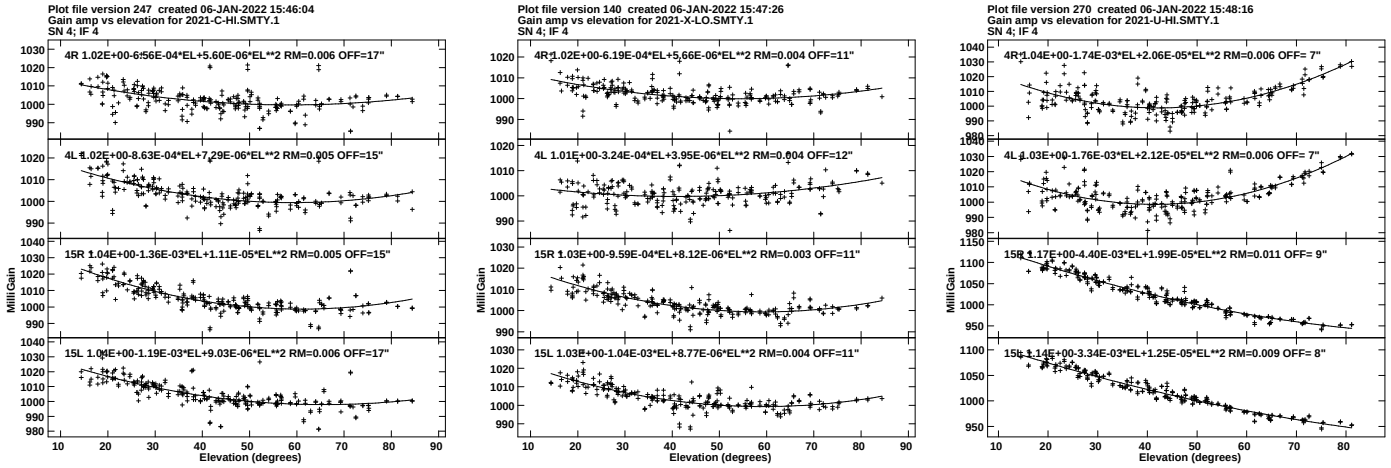

Figure 4: Showing the ELINT fits in R and L for antennas 4 (upper two) and 15 (lower two), at C, X, and Ku bands for a single SPW.

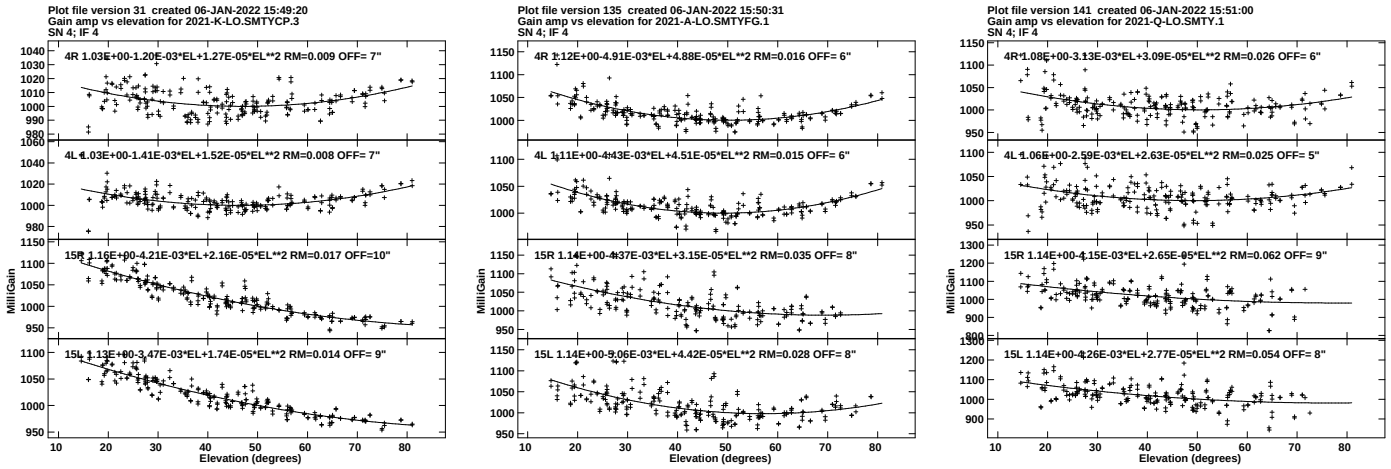

Figure 5: Showing the ELINT fits in R and L for antennas 4 and 15, at K, Ka, and Q bands for a single SPW.

remove the elevation dependency) are upward facing parabolas. At C-band, the higher IF shows a pattern similar to the higher frequency bands, but the lower IF does not. For this frequency band (and for L and S bands), any elevation dependency is not likely due to changes in antenna efficiency or optical misalignments, and is more likely due to some small elevation dependency in the electronics. In all cases, these discrepancies are very small, typically 1%.

In the following plots, (Figures 6 through 14), we show the gain curves for each of the 27 antennas (ea05 was out of the array), at the six highest frequency bands. It is important to note that these plots (except for Q-band) are the *averaged* solutions between the two IFs for each band. For each plot, the post-fit voltage gain rms is given in the index box, in the same units as the y-axis voltage gain. We have not attemped an error analysis, but note that the ~ 100 separate source observations utilized in the fit are statistically uncorrelated, so that the expected error in the derived gain curve could be up to an order of magnitude less than the values given in each box.

For Q-band, only the 42 GHz solutions are plotted, as the rapid increase in solution scatter at 48 GHz (due both to the pointing variations, and the decreased sensitivity) result in clearly inaccurate elevation gain solutions.

There is a wide (and astonishing) range of behaviors seen in these plots. Although the expected dominant effect – an upward facing parabola – is clearly present in most antennas, the expected (and hoped-for) minimization at an elevation near 50 degrees is not commonly seen. As expected, the gain curves for C and X bands are very flat – nearly always less than 1% in voltage correction.

As expected, the four high frequency bands show much larger elevation gain sensitivity. However, the gain

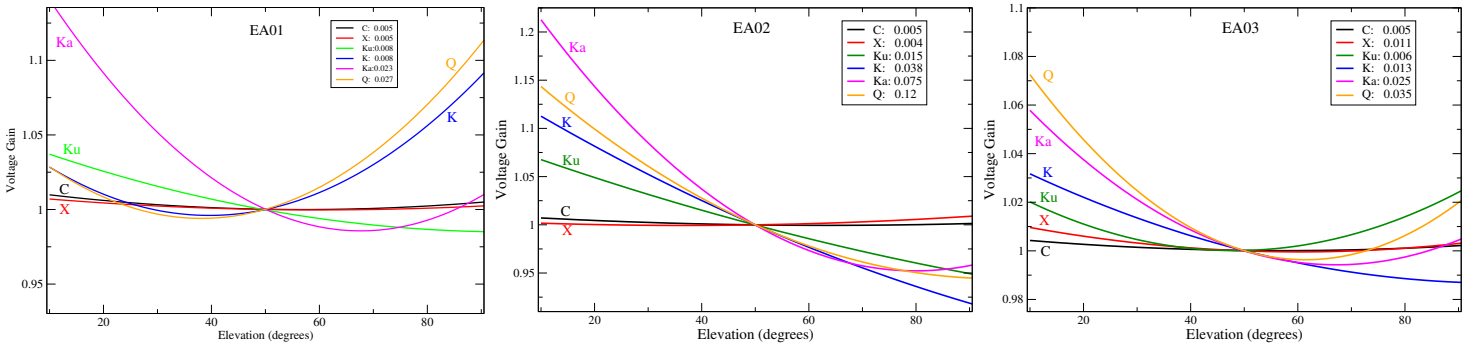

Figure 6: ELINT solutions for antennas 1, 2, and 3, from X through Q bands, normalized to 50 degrees.

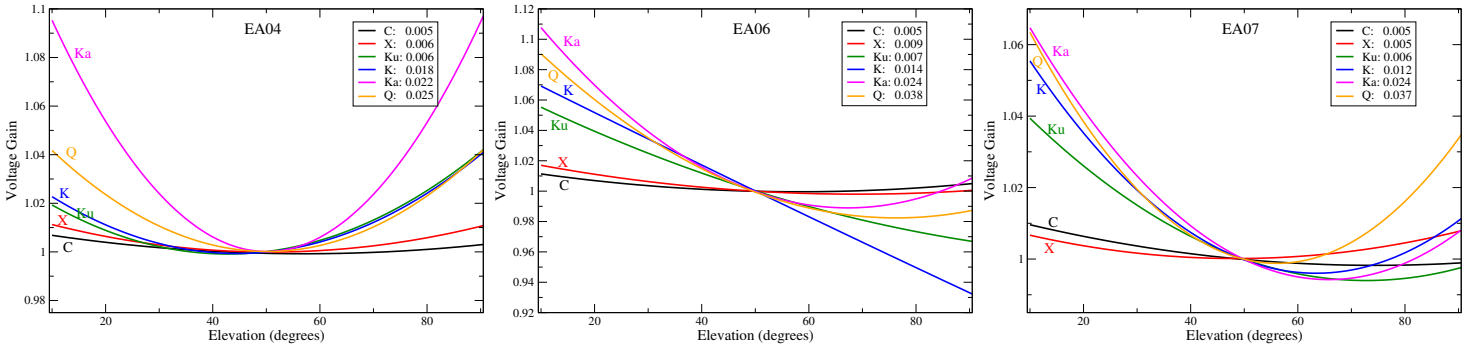

Figure 7: ELINT solutions for antennas 4, 6, and 7, from X through Q bands, normalized to 50 degrees.

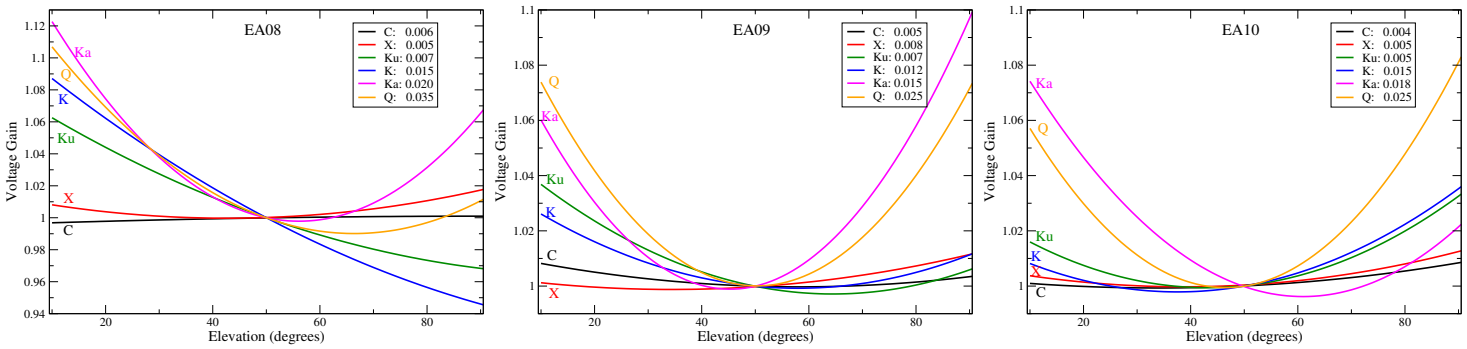

Figure 8: ELINT solutions for antennas 8, 9, and 10, from X through Q bands, normalized to 50 degrees.

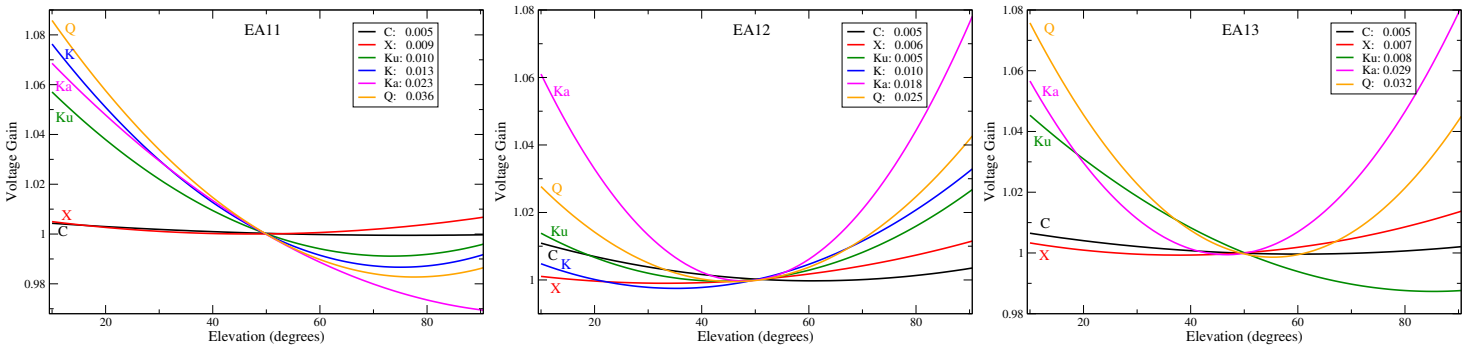

Figure 9: ELINT solutions for antennas 11, 12 and 13, from X through Q bands, normalized to 50 degrees.

parabolas are commonly different, and it is often the case that Ka-band shows the largest elevation sensitivity, commonly much larger than that of Q-band. Furthermore, the Ka-band curves show this band has in general

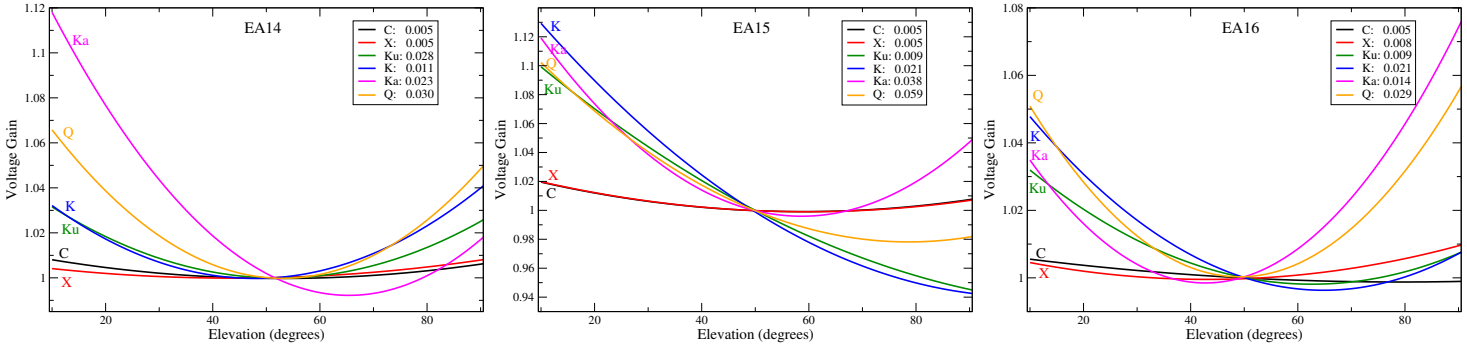

Figure 10: ELINT solutions for antennas 14, 15, and 16, from X through Q bands, normalized to 50 degrees.

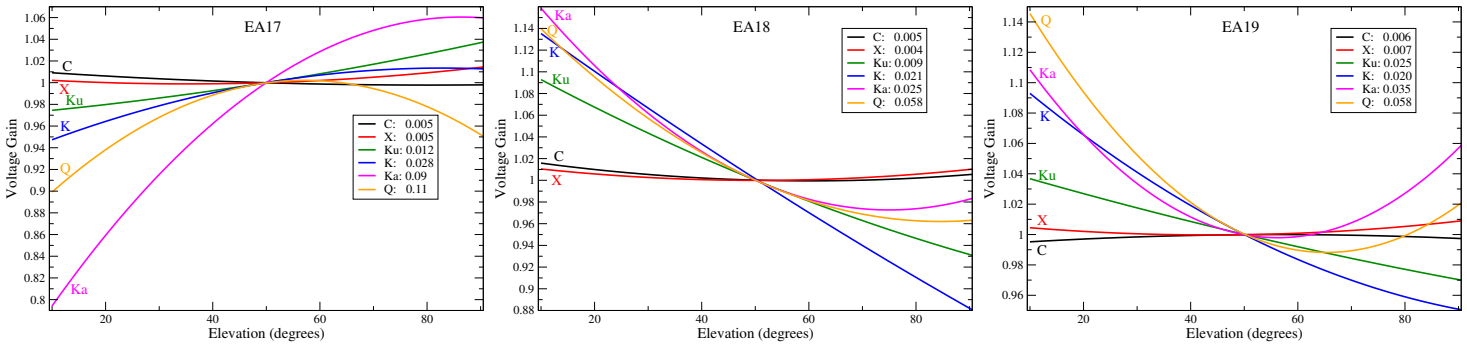

Figure 11: ELINT solutions for antennas 17, 18, and 19, from X through Q bands, normalized to 50 degrees.

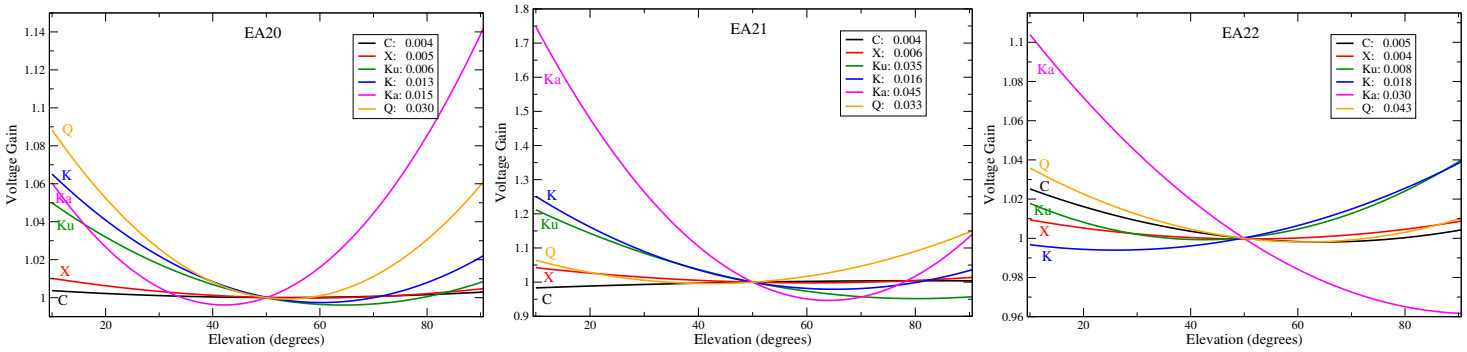

Figure 12: ELINT solutions for antennas 20, 21, and 22, from X through Q bands, normalized to 50 degrees.

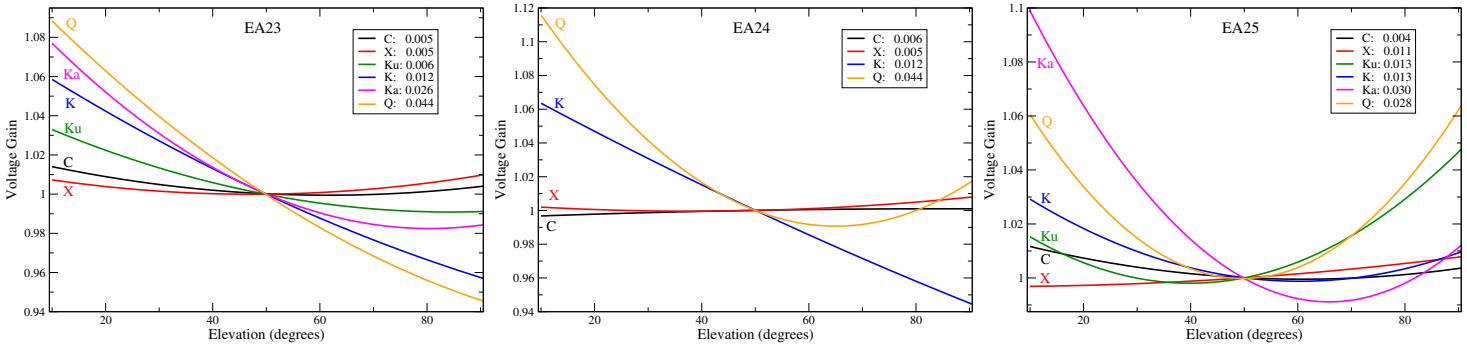

Figure 13: ELINT solutions for antennas 23, 24, and 25, from X through Q bands, normalized to 50 degrees.

the greatest elevation gain dependency – more than Q-band for most antennas.

The likely origin of these significantly varying gain results is optical alignment errors. The subreflector

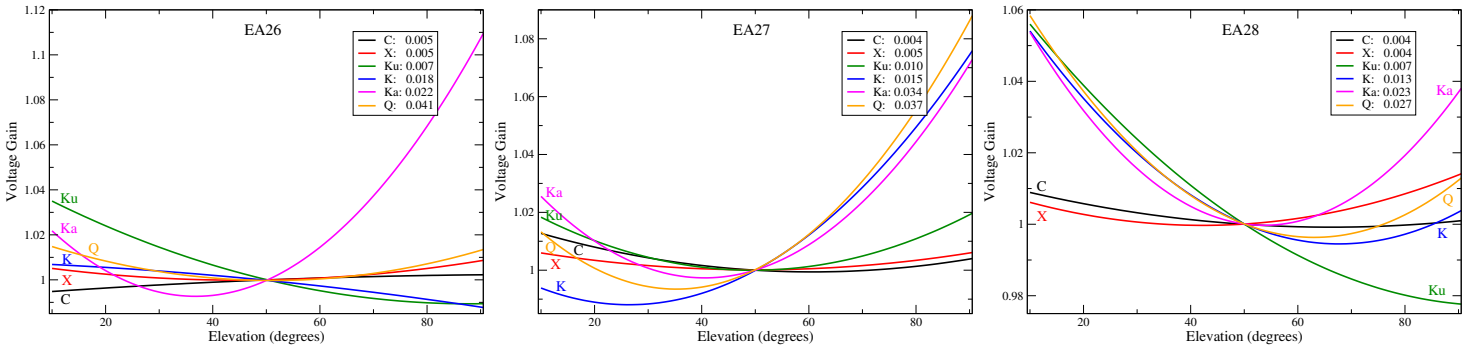

Figure 14: ELINT solutions for antennas 26, 27, and 28, from X through Q bands, normalized to 50 degrees.

rotation offsets described in EVLA Memo 211 cannot correct for horizontal subreflector positioning errors (which are clearly present), nor for positioning errors of the cassegrain feeds. The often dramatic differences in the gain curves between bands strongly suggests that feed positioning errors are largely responsible.

6 Intra-Band and Polarization Gain Gain Dependency

The preceding section shows the IF-averaged gain dependency on elevation. In all cases, the change in dependency over the 1-GHz-wide IF is very small (typically less than 1%). But what about between the band edges? Is an average of the two observed IFs, located near the edges of each band, a sufficient approximation for reasonable gain corrections for the entire band? If not, a frequency-dependent formulation will be required for elevation gain corrections. Similarly, are the gain curves for the two polarizations significantly different?

To answer these questions, the elevation gain curves for the two separate IF tunings for three bands, and nine antennas, have been plotted. Figs 15, 16 and 17 show the frequency dependencies across Ku, K, and Ka-bands.

For nearly all cases, the two polarizations have very similar gain curves, so there is no need to separately correct them. However, it is evident that there is an often significant change in gain corrections over the band, particularly for K and Ka bands. (The two Ku-band measurements, however, are relatively close in frequency, since the lowest 1.5 GHz of that band is significantly compromised by satellite RFI).

Is the change in the elevation gain within K and Ka bands sufficient to warrant the complication of putting in a frequency dependent correction? At the present, the answer is 'probably not', as the differential is generally within 1 to 2 percent – comparable to the error in the coefficients, and to the mean scatter in the gain determination.

7 Acknowledgements

Many thanks to Eric Greisen for his efforts in modifying AIPS tasks to better analyze and present these data, and to Ken Sowinski and Bryan Butler for comments on an earlier draft, and discussions over the many years we have been working on these issues.

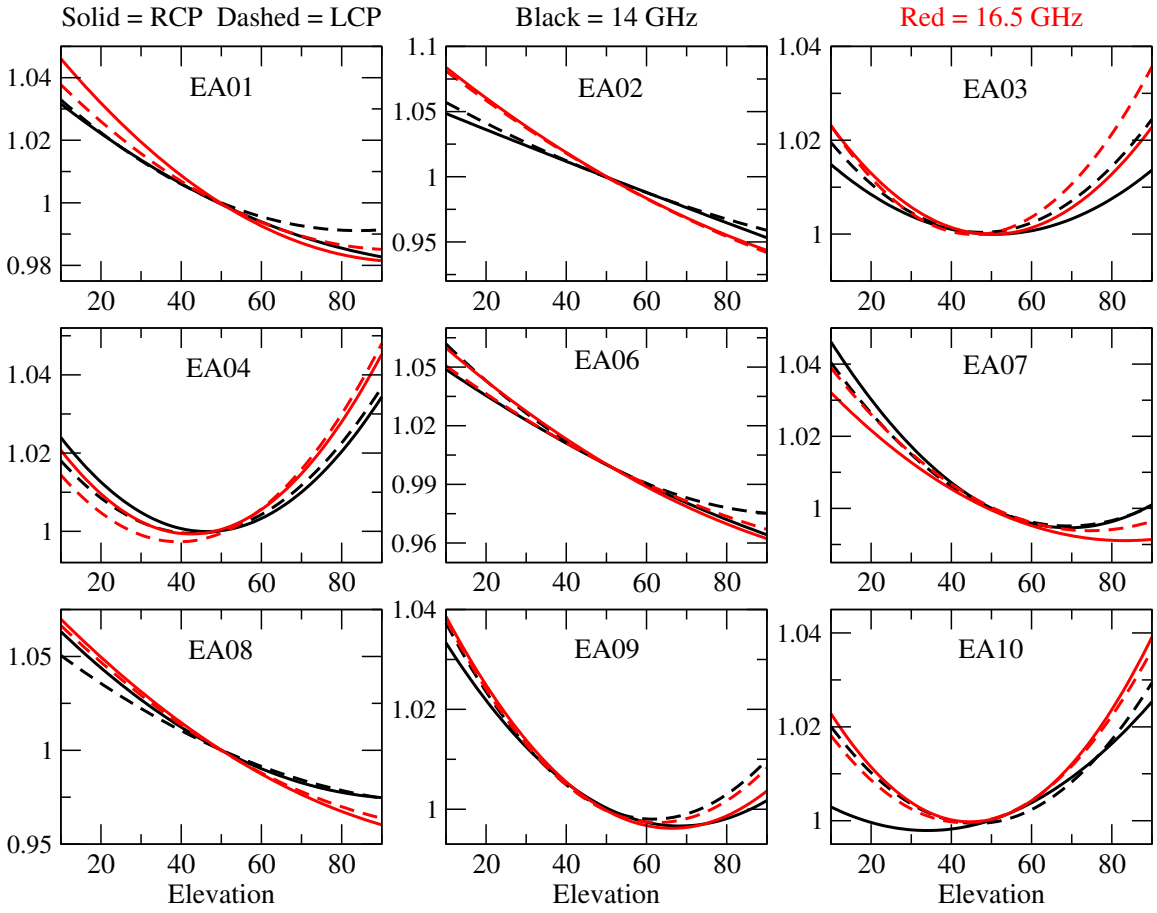

Figure 15: Showing the elevation-gain fits for Ku Band for nine antennas. Black curves are the R and L fits at 14 GHz, red curves show the fits at 16.5 GHz. The curves are very similar, but in general, the higher frequency has a sharper gain dependency.

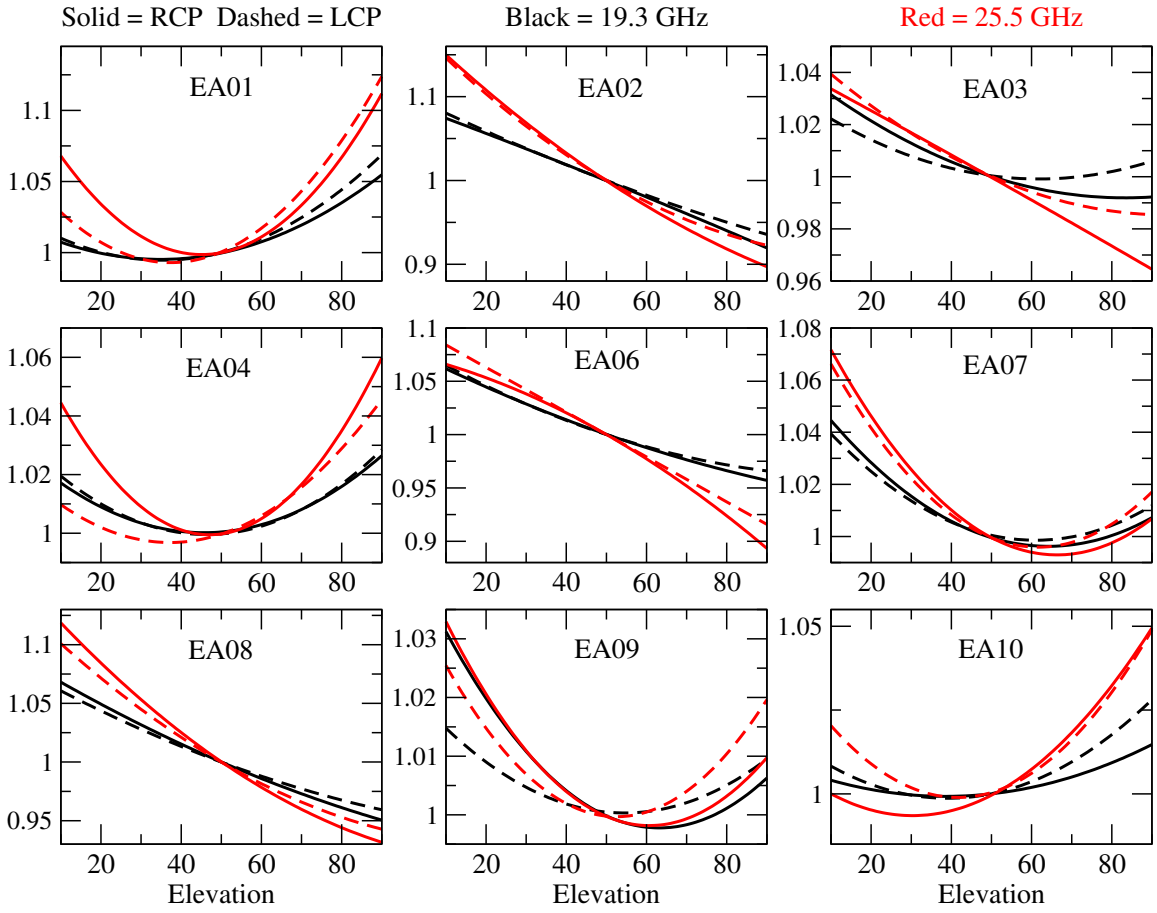

Figure 16: Showing the elevation-gain fits for K Band for nine antennas. Black curves are the R and L fits at 19.2 GHz, red curves show the fits at 25.5 GHz. The curves are generally similar, but in general, the higher frequency has a sharper gain dependency.

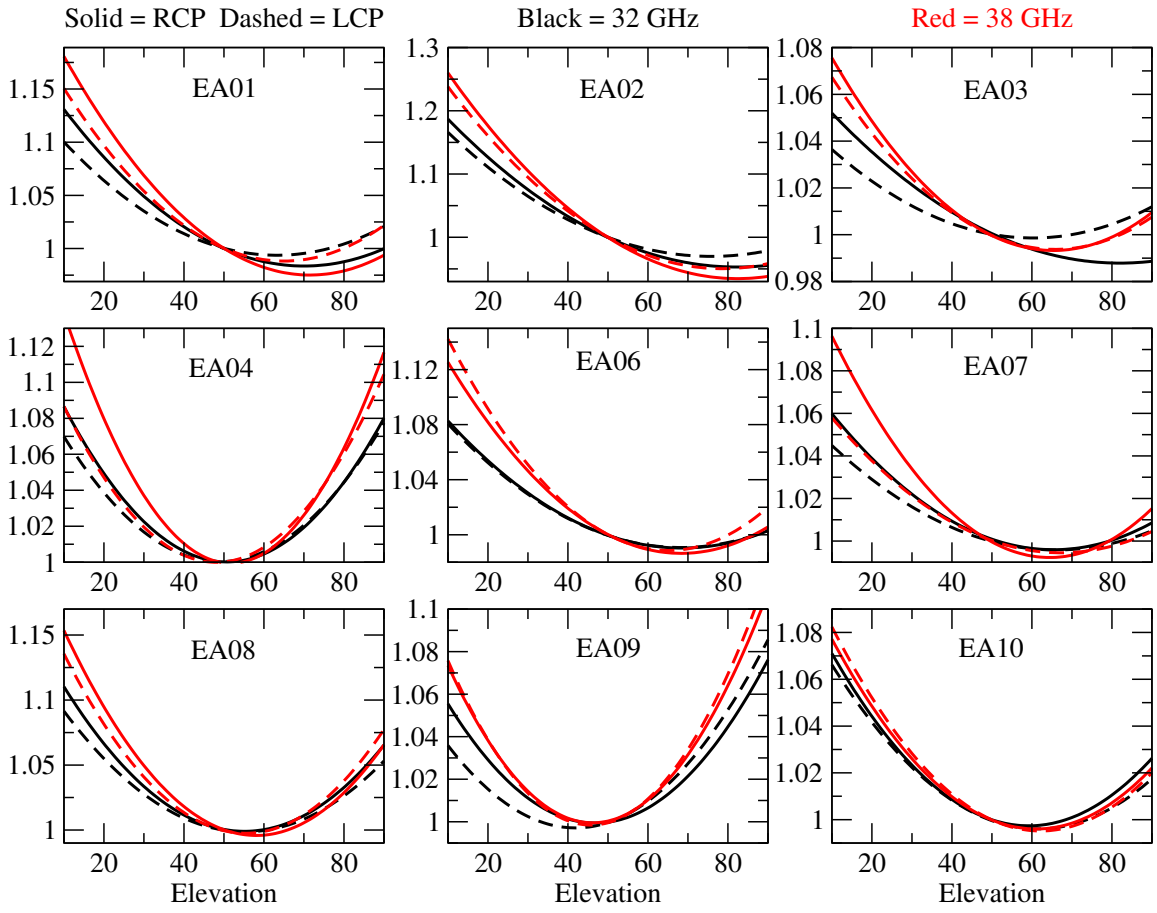

Figure 17: Showing the elevation-gain fits for Ka Band for nine antennas. Black curves are the R and L fits at 32 GHz, red curves show the fits at 37 GHz. The curves are very similar, but in general, the higher frequency has a sharper gain dependency.